2018

Evaluating an analytical model to predict subsurface LNAPL distributions and transmissivity from current and historic fluid levels in groundwater wells: Comparing results to numerical simulations

Robert J. Lenhard

Kaveh Sookhak Lari
Edith Cowan University

John L. Rayner

Greg B. Davis

10.1111/gwmr.12254
Lenhard, R. J., Sookhak Lari, K., Rayner, J. L., & Davis, G. B. (2018). Evaluating an analytical model to predict subsurface LNAPL distributions and transmissivity from current and historic fluid levels in groundwater wells: comparing results to numerical simulations. *Groundwater Monitoring & Remediation*, *38*(1), 75-84. Available here

Groundwater
Monitoring&Remediation

Evaluating an Analytical Model to Predict Subsurface LNAPL Distributions and Transmissivity from Current and Historic Fluid Levels in Groundwater Wells: Comparing Results to Numerical Simulations

by Robert J. Lenhard, Kaveh Sookhak Lari, John L. Rayner, and Greg B. Davis

Abstract

A recent analytical model predicts free, entrapped, and residual LNAPL saturations and the LNAPL transmissivity in the subsurface from current and historic fluid levels in groundwater wells. As such, the model accounts for effects of fluid level fluctuations in a well. The model was developed to predict LNAPL specific volumes and transmissivities from current fluid level measurements in wells and either recorded historic fluid level fluctuations in wells or estimates. An assumption is made in the model that the predictions are not dependent on whether the historic highest or lowest fluid level elevations in a well occur first. To test the assumption, we conduct two simulations with a modified multiphase flow numerical code TMVOC that incorporates relative permeability-saturation-capillary head relations employed in the model. In one simulation, the initial condition is for fluid levels in a well at the historic highest elevations. In the other simulation, the initial condition is for fluid levels in a well at the historic lowest elevations. We change the boundary conditions so both historical conditions occur followed by generating the current condition. Results from the numerical simulations are compared to model predictions and show the assumption in the analytical model is reasonable. The analytical model can be used to develop/refine conceptual site models and for assessing potential LNAPL recovery endpoints, especially on sites with fluctuating fluid levels in wells.

Introduction

The cleanup or remediation of light non-aqueous phase liquid (LNAPL) contaminated sites is still complex and challenging. Poorly planned and ill-conceived operations may increase potential risks to the public and environment. Remediation goals may be developed that are unachievable with selected technologies. Regardless, remediation of LNAPL contaminated sites can be onerous and expensive. From prior cleanup efforts and studies over time, remediation engineers and scientists have better understood LNAPL behavior in the subsurface and applied the knowledge to better remediate LNAPL contaminated sites. From the earlier conceptual models of LNAPL pancakes on top of water-bearing sediments to current understanding that LNAPL is variably saturated in the subsurface where the LNAPL can exist in free (mobile), entrapped, and residual forms, there has been significant progress. Understanding how all forms of LNAPL are distributed in the subsurface is fundamental to developing an effective LNAPL management strategy (US EPA 2004) as well as determining the potential risk to human health and the environment (CRC CARE 2015). The heterogeneous nature of subsurface strata further complicates LNAPL management strategies. There may be sharp discontinuities in LNAPL saturations across contrasting subsurface layers, i.e., fine-grained vs. coarse-grained layers or lens. The increased knowledge of subsurface LNAPL behavior also helps regulators in their efforts to minimize the risks from LNAPL contaminated sites while not imposing unreasonable conditions for regulatory site closure. However, more knowledge and improved predictive models are needed (Suthersan et al. 2016) to efficiently remediate sites and to assess risks to the public health and the environment. In some cases, complete LNAPL remediation may not be possible in reasonable time periods and costs. A critical component is assessing endpoints for active remediation activities. Thereafter, natural LNAPL attenuation may be the recommended path forward, provided public health and environmental risks are acceptable.

 doi: 10.1111/gwmr.12254

Although the general knowledge of subsurface LNAPL behavior has increased significantly over time, guidance by regulatory agencies concerning cleanup of LNAPL contamination has not changed as rapidly. In the United States, removal of LNAPL from the subsurface was addressed in regulations for underground storage tanks. The U.S. EPA developed the regulations in the late 1980s (US EPA 1988) where free product, or LNAPL, was defined as "a regulated substance that is present as a non-aqueous-phase liquid." In the regulations, Section 280.64 requires owners and operators to remove LNAPL from the subsurface to the maximum extent practicable as determined by the implementing agency, which would be individual states. Another requirement in Section 280.64 is the abatement of LNAPL migration into previously uncontaminated areas. In the preamble for the 40 CFR 280 regulations, the US EPA explains it was requiring removal of LNAPL to the maximum extent practicable instead of a specific metric because it wanted to give flexibility to implementing agencies in response to a comment recommending LNAPL only needed to be removed to a thickness of one eighth inch. (0.32 cm). By not including a specific metric for LNAPL removal, U.S. EPA was allowing implementing agencies to consider available technologies and site-specific conditions for assessing the maximum extent practicable. In the same preamble, however, the U.S. EPA decided to require devices capable of detecting the presence of at least one eighth inch (0.32 cm) of LNAPL on top of groundwater in monitoring wells for detecting the presence of LNAPL from underground storage tanks (Section 280.43(f)). The basis for the one eighth inch (0.32 cm) performance standard was because existing technology could sense one eighth inch (0.32 cm) of LNAPL on top of groundwater.

The "to the maximum extent practicable" United States standard for removing LNAPL from the subsurface posed issues for U.S. states in developing their regulations to be in compliance with the U.S. regulations. Individual states were left to make their own interpretations. Many of the states chose to include a metric to trigger the cleanup and closure of LNAPL contaminated sites. Because of the understanding of subsurface LNAPL behavior at the time, technology capabilities for removing LNAPL on top of groundwater in wells at the time, and/or the one eighth inch (0.32-cm) requirement for sensing LNAPL in monitoring wells in the U.S. regulations, a 0.01 foot (0.30 cm) LNAPL thickness in monitoring wells was adopted in some states guidance and regulations as a metric to which LNAPL needed to be removed before potential closure of sites. However, some U.S. states have/are amended/amending their guidance and regulations putting less emphasis on the 0.01 foot (0.30 cm) LNAPL thickness metric in monitoring wells, or removing the well-thickness metric completely, and placing more emphasis on LNAPL mobility and risks (MDEQ 2014). Some states have included guidance for using LNAPL transmissivity as a potential metric (VDEQ 2012; MDEQ 2014). Montana DEQ (2013) guidance recommends active LNAPL recovery (i.e., pumping from wells) whenever the LNAPL thickness in a well is in excess of 0.5 feet (15.2 cm). MassDEP (2016) guidance acknowledges the LNAPL thickness in a well is not a reliable indicator of the mobility or recoverability of LNAPL. The recent changes in guidance and regulations give regulators more flexibility for assessing potential closure of LNAPL contaminated sites. Typically criteria for site closure are assessing (1) LNAPL has been recovered to the "maximum extent practicable" (which may have different interpretations among U.S. states); (2) all risks have been assessed to be acceptable; and (3) institutional controls are placed on the land, if needed. Metrics related to the LNAPL thickness in wells, nevertheless, are still incorporated in some state guidance and regulations (NJDEP 2012; VDEQ 2012; Montana DEQ 2013; MassDEP 2016), even though there may be more recent guidance concerning LNAPL transmissivity.

Similar to the United States, individual Australian states regulate the cleanup and closure of LNAPL contaminated sites. Australian states, however, do not include a well thickness metric as a trigger for cleanup or for closure of sites. Typical criteria in Australia for either requiring LNAPL cleanup or closure of LNAPL contaminated sites are (1) whether the contamination poses unacceptable risks and (2) whether active remediation is practicable. However, most Australian states require management of contaminated LNAPL sites, irrespective of potential risk to public health and the environment, if free LNAPL exists in a well (CRC CARE 2015). The attainment of a remediation endpoint with LNAPL recovery is recognized as only one step of the remediation process and other steps may be required to meet statutory requirements (CRC CARE 2015).

To help practitioners and regulators assess whether a LNAPL contaminated site has been cleaned up "to the maximum extent practicable," more tools based on sound porous media physics are needed. Practitioners and regulators need to rely more on the current understanding of subsurface LNAPL physics, benefits of active LNAPL remediation technologies, and potential risks to public health and the environment than older concepts which may have been codified into guidance and regulations. In 1990, Farr et al. (1990) and Lenhard and Parker (1990a, 1990b) showed LNAPL saturations in the subsurface depend on capillary heads and are variable with depth, debunking the concept of LNAPL pancakes. All of the LNAPL in their models, however, were assumed to be mobile. Later, Charbeneau 2007 utilized the works of Parker et al. (1987), Farr et al. (1990), Lenhard and Parker (1990a), Parker et al. (1990, 1994), and Waddill and Parker (1997) to develop the LDRM model, which considered residual LNAPL entrapped by water (water occluded) below the water table and residual LNAPL above the water-saturated region. The LDRM model has been used by practitioners and regulators to develop subsurface LNAPL conceptual models and management plans. The residual saturations were assumed to be constant below the water-saturated region and constant above the water-saturated region with the residual saturation in the water-saturated region typically larger than that above the water-saturated region (Charbeneau 2007, Figures 3-2). The residual LNAPL is assumed to be immobile. The mobile LNAPL is determined from the difference between the total and residual LNAPL saturations.

Recently, Lenhard et al. (2017) extended the model of Lenhard and Parker (1990a) to include elevation-dependent entrapped and residual LNAPL, where the residual LNAPL is defined as in Lenhard et al. (2004) (i.e., LNAPL above the

water-saturated zone in films, pore wedges, and bypassed pores, which is relatively immobile). By integrating the LNAPL saturations over depth, Lenhard et al. (2017) predict LNAPL volumes and transmissivities (both total and recoverable) for a vertical slice of the subsurface. The LNAPL transmissivities are based on the free (mobile) LNAPL saturations after considering the variable, elevation-dependent, entrapped, and residual LNAPL saturations. The LNAPL transmissivity is a measure of LNAPL mobility over the depth of the subsurface where free LNAPL is present. According to ASTM (2013), LNAPL transmissivity is an accurate metric for understanding LNAPL recovery. In addition, Lenhard et al. (2017) accounts for fluctuations of the fluid levels in wells over time on the current distribution of LNAPL (free, entrapped, and residual) in the subsurface. From the current elevations of the air-LNAPL and LNAPL-water interfaces in wells, the historical highest air-LNAPL interface elevation, and the historical lowest LNAPL-water interface elevation, Lenhard et al. (2017) predicts the current free, entrapped, and residual LNAPL saturations with elevation and the corresponding elevation-dependent LNAPL relative permeabilities. In developing their predictions, they assumed the current LNAPL saturation distributions are not dependent on whether the historical highest air-LNAPL interface or the historical lowest LNAPL-water interface occurred first. The model is an advancement on better understanding LNAPL distributions in the subsurface and the potential mobility of the LNAPL. Practitioners and regulators can use the model, which is a simple tool, to more accurately assess the current LNAPL distribution in the subsurface and its potential mobility. The model also can be used to continually update the conceptual site model of LNAPL contaminated sites, which is used to guide remediation strategy and activities, as the fluid levels in wells change over time.

In this paper, we will investigate whether the assumption made in Lenhard et al. (2017) that predicted free, entrapped, and residual LNAPL saturations from the model will be similar whether the historical highest or lowest fluid levels in monitoring wells occurred first. To conduct the investigation, we compare numerical simulations of changes in LNAPL saturations as subsurface conditions vary between the historic highest and lowest air-LNAPL and LNAPL-water levels in a monitoring well prior to the current air-LNAPL and LNAPL-water levels in the well. In one simulation, the initial conditions are fluid heads corresponding to the historic highest air-LNAPL and LNAPL-water levels in the well. In another simulation, the initial conditions are fluid heads corresponding to the historic lowest air-LNAPL and LNAPL-water levels in the well. To conduct the simulations, we modified a commercially available multiphase flow numerical code to utilize the same constitutive relations between capillary heads, fluid saturations, and relative permeabilities as in Lenhard et al. (2017). The multiphase flow numerical code is TMVOC (Pruess and Battistelli 2002). We compare simulations using the modified TMVOC to predictions from the Lenhard et al. (2017) model for a hypothetical, LNAPL-contaminated, homogeneous porous medium. The comparisons between free, entrapped, and residual LNAPL saturations in the subsurface from the numerical simulations and the Lenhard et al. (2017) model will be used to test the assumption in the model. The purpose is to investigate whether the Lenhard et al. (2017) analytical model, which is simpler tool than sophisticated numerical models, provides comparable predictions as numerical models for developing or refining site conceptual models of LNAPL contamination and assessing potential LNAPL mobility.

Numerical Model Modification

The source code for the multiphase, multicomponent TMVOC software, which is a FORTRAN 77 integral finite-difference simulator, is commercially available containing subroutines with simple constitutive relations for fluid relative permeabilities, saturations, and capillary heads. The Commonwealth Scientific and Industrial Research Organization (CSIRO), an Australian Government corporate entity, purchased, modified, and used the multiphase, multicomponent TMVOC to investigate subsurface contamination issues with LNAPL (Sookhak Lari et al. 2016a, 2016b; Lekmine et al. 2017). To conduct numerical simulations of LNAPL saturation distributions to test the assumption in the Lenhard et al. (2017) model, we modified subroutines in TMVOC to incorporate equivalent relative permeability-saturation-capillary head constitutive relations in Lenhard et al. (2017).

Saturation–Capillary Head Relations

In Lenhard et al. (2017), the apparent total liquid ($\overline{\overline{S}}_t$) and apparent water ($\overline{\overline{S}}_w$) saturations are functions of the air-LNAPL (h_{ao}) and LNAPL-water (h_{ow}) capillary heads, respectively

$$\overline{\overline{S}}_t = f\left(\beta_{ao} h_{ao}\right) \tag{1}$$

$$\overline{\overline{S}}_w = f\left(\beta_{ow} h_{ow}\right) \tag{2}$$

where β_{ao} and β_{ow} are air-LNAPL and LNAPL-water scaling factors, respectively, which are ratios of interfacial tensions calculated as

$$\beta_{ao} = \frac{\sigma_{ao} + \sigma_{ow}}{\sigma_{ao}} \tag{3}$$

$$\beta_{ow} = \frac{\sigma_{ao} + \sigma_{ow}}{\sigma_{ow}} \tag{4}$$

where σ_{ao} and σ_{ow} are the air-LNAPL and LNAPL-water interfacial tensions, respectively.

Using the van Genuchten (1980) function to describe relations between fluid saturations and capillary heads, the apparent total liquid and water saturations can be determined following Parker et al. (1987) as

$$\overline{\overline{S}}_t = \left[1 + \left(\beta_{ao}\alpha h_{ao}\right)^n\right]^{-m} \tag{5}$$

$$\overline{\overline{S}}_w = \left[1 + \left(\beta_{ow}\alpha h_{ow}\right)^n\right]^{-m} \tag{6}$$

where α and n are van Genuchten parameters for an air-water fluid system in which

$$m = 1 - 1/n \tag{7}$$

The apparent total liquid saturation is defined as

$$\overline{\overline{S}}_t = \frac{S_o + S_w - S_{wr}}{1 - S_{wr}} \tag{8}$$

where S_o, S_w, and S_{wr} are the actual LNAPL, water, and residual water saturations, respectively. The apparent total liquid saturation was defined originally by Parker and Lenhard (1987) to include entrapped air by either water or LNAPL, but Lenhard et al. (2017) neglected entrapped air to simplify the development of their model.

The apparent water saturation is defined as

$$\overline{\overline{S}}_w = \frac{S_w + S_{oe} - S_{wr}}{1 - S_{wr}} \tag{9}$$

where S_{oe} is the actual entrapped LNAPL saturation (i.e., LNAPL occluded by water as ganglia above or in the water-saturated subsurface). As with the apparent total liquid saturation, Lenhard et al. (2017) neglected entrapped air from the original definition given by Parker and Lenhard (1987).

In Lenhard et al. (2017), the actual total LNAPL saturation has three forms or elements: free (mobile), entrapped, and residual.

$$S_o = S_{of} + S_{oe} + S_{or} \tag{10}$$

where S_{of}, S_{oe}, and S_{or} are the actual free (mobile), entrapped, and residual LNAPL saturations. The residual LNAPL saturation consists of LNAPL above the water-saturated zone in films, pore wedges, and bypassed pores (not water occluded LNAPL resulting from water imbibition).

Following Lenhard et al. (2004), the residual LNAPL saturation can be determined from the current time step apparent water saturation ($\overline{\overline{S}}_w$), the historical largest apparent total liquid saturation ($\overline{\overline{S}}_t^{max}$), and a calibration term (S_{or}^{max}) representing the maximum actual residual LNAPL saturation for the porous medium.

$$S_{or} = S_{or}^{max}\left(\overline{\overline{S}}_t^{max} - \overline{\overline{S}}_w\right)^{0.5}\left(1 - \overline{\overline{S}}_w\right)^{1.5} \tag{11}$$

A method to determine S_{or}^{max}, which is a constant, is described in Lenhard et al. (2004); it is porous medium and LNAPL specific. $\overline{\overline{S}}_t^{max}$ is a variable for each node that must be updated after convergence of each time step. Whenever the converged current time step $\overline{\overline{S}}_t$ is greater than $\overline{\overline{S}}_t^{max}$, then $\overline{\overline{S}}_t^{max}$ is updated to equal the current time step $\overline{\overline{S}}_t$. $\overline{\overline{S}}_w$ is determined from each iteration of a time step. Equation 11 was tested in numerical simulations by Oostrom et al. (2005) and shown to yield accurate predictions of LNAPL saturations of transient flow experiments.

Lenhard et al. (2017) calculated the actual entrapped LNAPL saturation (water occluded LNAPL above or in the water-saturated zone) from the current time step apparent water saturation ($\overline{\overline{S}}_w$), the historical smallest apparent water saturation ($\overline{\overline{S}}_w^{min}$), and a calibration term (S_{oe}^{max}) representing the maximum actual entrapped LNAPL saturation for the porous medium.

$$S_{oe} = S_{oe}^{max}\left(\overline{\overline{S}}_w - \overline{\overline{S}}_w^{min}\right) \tag{12}$$

A method to determine S_{oe}^{max}, which is a constant, is measuring the actual entrapped LNAPL saturation resulting from water imbibition into an initially LNAPL-saturated porous medium until it is apparently water saturated, which is porous medium and LNAPL specific. $\overline{\overline{S}}_w^{min}$ is also a variable for each node that must be updated after convergence of each time step.

The actual free (mobile) LNAPL saturation can be determined from

$$S_{of} = \left(1 - S_{wr}\right)\left(\overline{\overline{S}}_t - \overline{\overline{S}}_w\right) - S_{or} \tag{13}$$

and the actual total LNAPL saturation (S_o) can be calculated from Equation 10 after S_{or}, S_{oe}, and S_{of} are computed.

Saturation–Permeability Relations

The LNAPL and water relative permeabilities are functions of saturations. In Lenhard et al. (2017), the LNAPL relative permeability is a function of the apparent total liquid ($\overline{\overline{S}}_t$) saturation, the apparent water ($\overline{\overline{S}}_w$) saturation, the effective free LNAPL ($\overline{S}_{of}$) saturation, and the effective residual LNAPL ($\overline{S}_{or}$) saturation, where

$$\overline{S}_{of} = \frac{S_{of}}{1 - S_{wr}} \tag{14}$$

$$\overline{S}_{or} = \frac{S_{or}}{1 - S_{wr}} \tag{15}$$

The LNAPL relative permeability is calculated as

$$k_{ro} = \overline{S}_{of}^{0.5}\left\{\frac{\int_{\overline{\overline{S}}_w + \overline{S}_{or}}^{\overline{\overline{S}}_t} \frac{d\overline{S}}{h\left(\overline{S}\right)}}{\int_0^1 \frac{d\overline{S}}{h\left(\overline{S}\right)}}\right\}^2 \tag{16}$$

where $\overline{S}$ is the effective porosity in which the flow of the fluid under consideration can potential occur and $h(\overline{S})$ is a surrogate for the pore-size distribution of the porous medium, which is the inverse of the van Genuchten (1980) function. The resulting expression for the LNAPL relative permeability is

$$k_{ro} = \overline{S}_{of}^{0.5}\left\{\left[1 - \left(\overline{\overline{S}}_w + \overline{S}_{or}\right)^{1/m}\right]^m - \left(1 - \overline{\overline{S}}_t^{1/m}\right)^m\right\}^2 \tag{17}$$

The water relative permeability is a function of the apparent water ($\overline{\overline{S}}_w$) saturation, the effective water ($\overline{S}_w$) saturation, and the effective entrapped LNAPL ($\overline{S}_{oe}$) saturation where

$$\overline{S}_w = \frac{S_w - S_{wr}}{1 - S_{wr}} \tag{18}$$

$$\overline{S}_{oe} = \frac{S_{oe}}{1 - S_{wr}} \tag{19}$$

Following Lenhard and Parker (1987), the water relative permeability is calculated as

$$k_{rw} = \overline{S}_w^{\,0.5} \left\{ \frac{\int_0^{\overline{\overline{S}}_w} \frac{d\overline{S}}{h\left(\overline{S}\right)} - \int_0^{\overline{S}_{oe}} \frac{d\overline{S}}{h\left(\overline{S}\right)}}{\int_0^1 \frac{d\overline{S}}{h\left(\overline{S}\right)}} \right\}^2 \tag{20}$$

yielding

$$k_{rw} = \overline{S}_w^{\,0.5} \left[1 - \left(1 - \frac{\overline{S}_{or}}{1 - \overline{\overline{S}}_w^{\,min}} \right) \left(1 - \overline{\overline{S}}_w^{\,1/m} \right)^m - \frac{\overline{S}_{or}}{1 - \overline{\overline{S}}_w^{\,min}} \left(1 - \overline{\overline{S}}_w^{\,min\,1/m} \right)^m \right]^2 \tag{21}$$

which is Equation (14c) in Lenhard and Parker (1987). For the LNAPL specific volume and transmissivity model of Lenhard et al. (2017), a water relative permeability is not required, but it is needed for conducting numerical simulations with TMVOC.

In addition to the water relative permeability, the gas-phase relative permeability is needed for conducting numerical simulations with TMVOC. Following Lenhard and Parker (1987), the gas-phase relative permeability is a function of the apparent total liquid ($\overline{\overline{S}}_t$) saturation and the effective gas ($\overline{S}_g$) saturation where

$$\overline{S}_g = 1 - \overline{\overline{S}}_t = \frac{S_g}{1 - S_{wr}} \tag{22}$$

in which S_g is the actual gas saturation. The gas-phase relative permeability is calculated as

$$k_{rg} = \overline{S}_g^{\,0.5} \left\{ \frac{\int_{\overline{\overline{S}}_t}^1 \frac{d\overline{S}}{h\left(\overline{S}\right)}}{\int_0^1 \frac{d\overline{S}}{h\left(\overline{S}\right)}} \right\}^2 \tag{23}$$

yielding.

$$k_{rg} = \overline{S}_g^{0.5} \left(1 - \overline{\overline{S}}_t^{\,1/m} \right)^{2m} \tag{24}$$

Table 1

Parameters Used in the Model and Simulations

Parameters	Values
van Genuchten α	0.124/cm
van Genuchten n	2.28 (–)
S_{wr}	0.139 cm^3/cm^3
Porosity	0.41 cm^3/cm^3
Water-saturated hydraulic conductivity	350 cm/day
$S_{or}^{\,max}$	0.15 cm^3/cm^3
$S_{oe}^{\,max}$	0.20 cm^3/cm^3
σ_{ow}	29 mN/m
σ_{ao}	36 mN/m
ρ_{ro}	0.73 (–)
Viscosity ratio (LNAPL to water)	0.8 (–)

which is Equation (18) in Lenhard and Parker (1987). Because entrapped gas is neglected by Lenhard et al. (2017), the effective gas saturation (Equation 22) is substituted for the effective free gas saturation in Lenhard and Parker (1987).

The relative permeability-saturation-capillary head relations were implemented in TMVOC to conduct simulations of LNAPL distributions resulting from changes of fluid levels in wells. The constitutive relations can be easily implemented in multiphase, multicomponent numerical simulators to better study the subsurface dynamics and partitioning of LNAPLs.

Model and Simulation Results

In this section, we compare results from the Lenhard et al. (2017) model to the one-dimensional simulations from TMVOC using parameters reflective of a homogeneous, sandy porous medium (see Table 1). The same parameter values are used in the analytical and numerical models. The parameters are also the same as those in Lenhard et al. (2017) study, except for the maximum actual entrapped LNAPL saturation. For simplicity, we will refer to the Lenhard et al. (2017) model as the model and refer to TMVOC simulations as the simulations.

Important inputs to the analytical model are elevations of fluid levels in wells. To model fluid behavior with TMVOC, the fluid heads in porous media need to correspond to the fluid levels in wells so appropriate boundary conditions can be imposed for the simulations. At vertical equilibrium conditions, the LNAPL head (h_o) is determined from

$$h_o = Z_{ao} - Z \tag{25}$$

and the water head (h_w) from

$$h_w = \rho_{ro} Z_{ao} + \left(1 - \rho_{ro}\right) Z_{ow} - Z \tag{26}$$

where Z_{ao} is the elevation of the air-LNAPL interface in a well, Z_{ow} is the elevation of the LNAPL-water interface in a well, Z is the elevation being evaluated, and ρ_{ro} is the LNAPL specific gravity (ratio of LNAPL to water mass density). The gas-phase head is always assumed to be atmospheric, i.e., zero. The LNAPL and water heads corresponding to the historic fluid levels in the well can be determined by

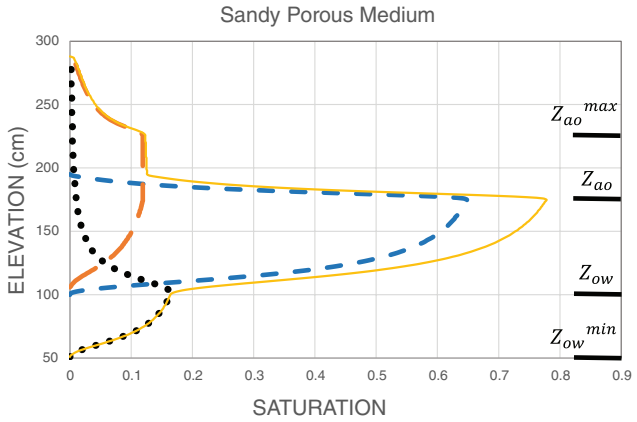

Figure 1. Predicted free (shorter broken blue line), residual (longer broken orange line), entrapped (dotted black line), and total (solid yellow line) LNAPL saturations as a function of elevation from the model. Elevations of the fluid levels in a well are marked on the right.

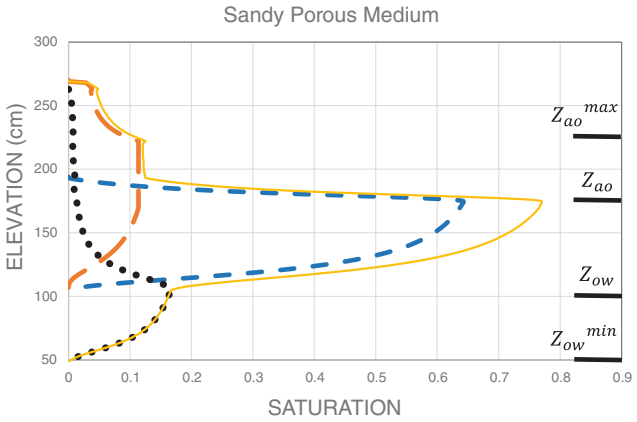

Figure 2. Predicted free (shorter broken blue line), residual (longer broken orange line), entrapped (dotted black line), and total (solid yellow line) LNAPL saturations as a function of elevation from Simulation Low. Elevations of the fluid levels in a well are marked on the right.

substituting Z_{ao} and Z_{ow} by the historic elevations in Equations 25 and 26.

Using the parameters in Table 1 and assuming the current elevation of the air-LNAPL interface in a well (Z_{ao}) is at 175 cm, the corresponding current elevation of the LNAPL-water interface (Z_{ow}) is at 100 cm (i.e., LNAPL thickness of 75 cm), the historical highest elevation of the air-LNAPL interface (Z_{ao}^{max}) was at 225 cm, and the historical lowest elevation of the LNAPL-water interface (Z_{ow}^{min}) was at 50 cm (fluid level fluctuations of 50 cm in each direction of current levels), the current predicted LNAPL distributions in the subsurface for the model is shown in Figure 1. The predictions assume the LNAPL did not infiltrate from the surface at the site. The spread (smear) of LNAPL vertically is because of fluid level fluctuations in the subsurface. The resulting predicted total LNAPL specific volume in a vertical slice of the subsurface is 26.25 cm^3/cm^2. The predicted free LNAPL specific volume is 16.59 cm^3/cm^2. The LNAPL distributions in Figure 1 will be compared later to the simulations.

The initial conditions for the simulations, which used the same parameters in Table 1, were developed by imbibing LNAPL into an air-water system. As LNAPL imbibed, the upper water-saturated elevation (i.e., the corresponding LNAPL-water interface in a well) lowered. LNAPL imbibition was stopped after the LNAPL specific volume was 26.25 cm^3/cm^2 (the amount of total LNAPL predicted by the model) and the upper water-saturated elevation was at either 50 or 150 cm. The 50-cm elevation is Z_{ow}^{min} and the 150-cm elevation is the elevation of the LNAPL-water interface when the air-LNAPL interface was at the historical highest elevation of 225 cm in the model (Z_{ao}^{max}), assuming a 75-cm LNAPL thickness in a well. In order to use the model with limited information (i.e., knowledge of current fluid level elevations in a well and estimates of historic water table fluctuations), the LNAPL thickness in the well at the historic fluid level fluctuations were assumed to be the same as the current LNAPL thickness.

For the simulation which began from initial conditions corresponding to the historical lowest fluid levels in a well, we refer to as Simulation Low. After the initial conditions

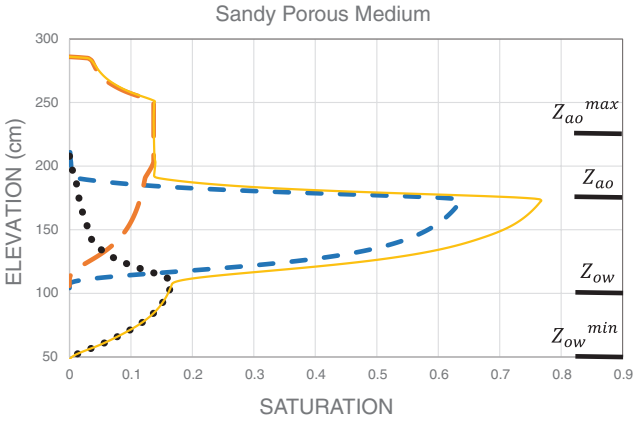

Figure 3. Predicted free (shorter broken blue line), residual (longer broken orange line), entrapped (dotted black line), and total (solid yellow line) LNAPL saturations as a function of elevation from Simulation High. Elevations of the fluid levels in a well are marked on the right.

were created, the boundary conditions were changed to reflect the LNAPL-water interface in a well going from the 50-cm elevation (Z_{ow}^{min}) to the 150-cm elevation, which corresponds to the air-LNAPL interface at the 225-cm elevation (Z_{ao}^{max}) in the model (i.e., the historical highest levels). After static conditions were approached, the boundary conditions were changed so the fluid levels in a well would decrease to current elevations (Z_{ao} = 175 cm and Z_{ow} = 100 cm).

For the simulation which began corresponding to the historical highest fluid levels in a well, we refer to as Simulation High. After the initial conditions were created, the boundary conditions were changed to reflect the LNAPL-water interface in a well going from the 150-cm elevation to the 50-cm elevation (Z_{ow}^{min}). After static conditions were approached, the boundary conditions were changed so the fluid levels in a well would rise to current elevations (Z_{ao} = 175 cm and Z_{ow} = 100 cm).

The current predicted LNAPL distributions in the subsurface for Simulation Low and Simulation High are shown in Figures 2 and 3, respectively. There appears to

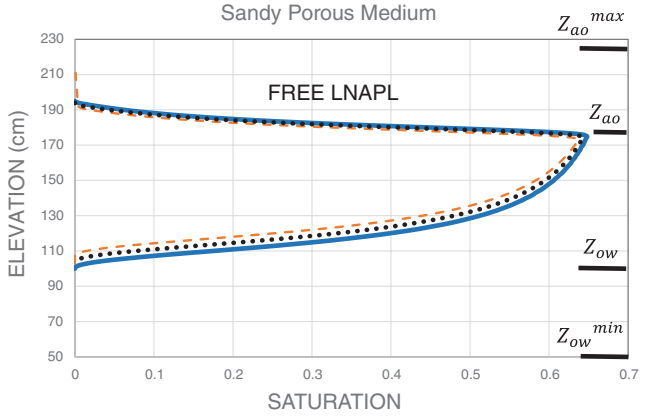

Figure 4. Predicted free LNAPL saturations from the model (solid blue line), Simulation Low (dotted black line), and Simulation High (broken orange line). Elevations of the fluid levels in a well are marked on the right.

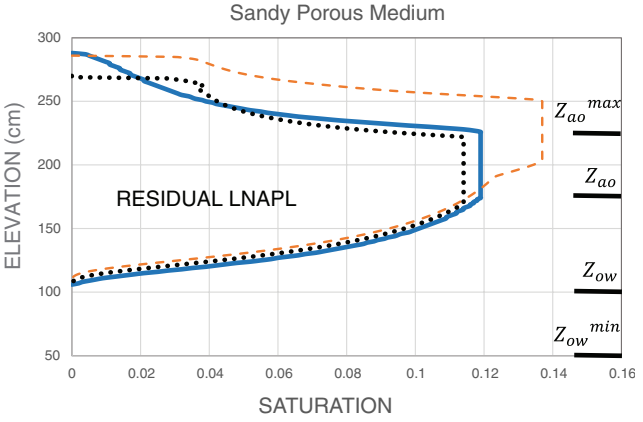

Figure 6. Predicted residual LNAPL saturations from the model (solid blue line), Simulation Low (dotted black line), and Simulation High (broken orange line). Elevations of the fluid levels in a well are marked on the right.

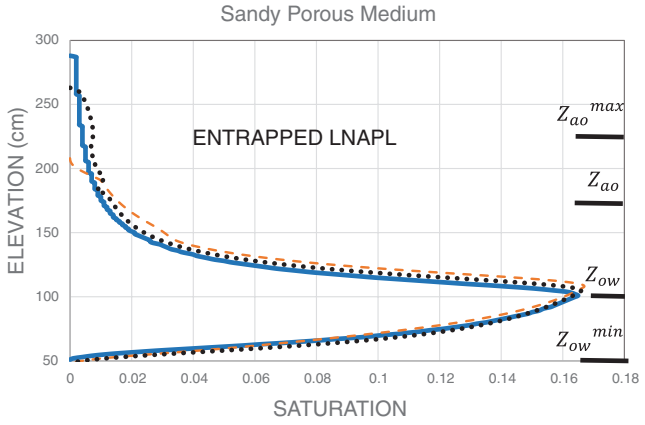

Figure 5. Predicted entrapped LNAPL saturations from the model (solid blue line), Simulation Low (dotted black line), and Simulation High (broken orange line). Elevations of the fluid levels in a well are marked on the right.

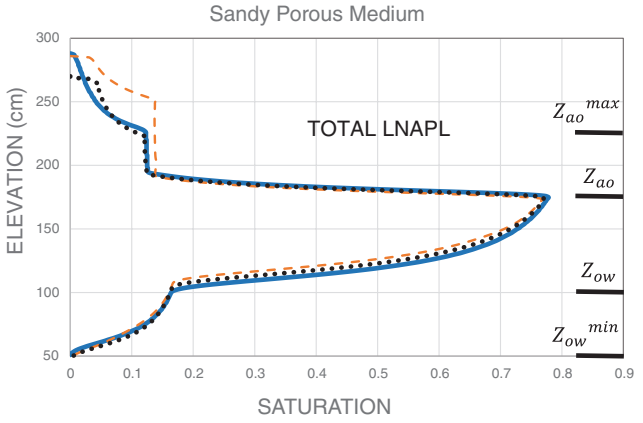

Figure 7. Predicted total LNAPL saturations from the model (solid blue line), Simulation Low (dotted black line), and Simulation High (broken orange line). Elevations of the fluid levels in a well are marked on the right.

be only slight differences among the simulations and the predicted LNAPL distributions from the model (Figure 1). To show the differences in greater detail, the predicted free, entrapped, residual, and total LNAPL distributions from the model, Simulation Low, and Simulation High are compared in Figures 4 to 7, respectively.

In Figure 4, the predicted free LNAPL saturations from the model and the simulations are similar. This suggests the predicted free LNAPL relative permeabilities and transmissivity from the model would closely match those determined from TMVOC (i.e., Simulation Low and Simulation High), because the same saturation-relative permeability relations are implemented in the model and TMVOC. Similar free LNAPL specific volumes also would be predicted from the model and TMVOC.

In Figure 5, the predicted entrapped LNAPL saturations from the model and the simulations also are similar, except for very low saturations at higher elevations. The majority of the entrapped LNAPL is in the water-saturated zone. Nevertheless, there is entrapped LNAPL above the water-saturated zone because water is on an imbibition path at current conditions relative to the historical lowest water saturations, which likely has displaced LNAPL into larger pore spaces entrapping LNAPL in the process. The amount of entrapped LNAPL, however, decreases significantly with distance above the water-saturated zone.

In Figure 6, the predicted residual LNAPL saturations from the model and the simulations are different above Z_{ao}. While the residual LNAPL predictions from the model and Simulation Low are relatively close, they are different than predictions from Simulation High. This is because of how initial conditions were created for the simulations. Initially, the LNAPL volume injected into the subsurface was the total LNAPL volume from the model (26.25 cm^3/cm^2), which consisted of free, entrapped, and residual LNAPL. This caused the equivalent LNAPL thickness in the well to be slightly greater than 75 cm at initial conditions. Therefore, there was a greater amount of LNAPL available (i.e., $\bar{\bar{S}}_t^{max} - \bar{\bar{S}}_w$) at the beginning of Simulation High, which led to larger predictions of residual LNAPL, particularly at the higher elevations. Nevertheless, the maximum

actual residual LNAPL saturation from Simulation High is less than 0.02 higher than that predicted by the model. The larger residual LNAPL saturations predicted by Simulation High at the higher elevations is somewhat offset by the lower residual LNAPL saturations at lower elevations. The majority of the residual LNAPL is in the unsaturated zone above Z_{ao}. The differences between the model and Simulation High predicted residual LNAPL saturations does not affect the predicted LNAPL transmissivity because the predicted free LNAPL saturations from the model and the simulations are similar (Figure 4).

In Figure 7, predicted total LNAPL saturations from the model and the simulations are similar, except at the highest elevations because of the differences in predicted residual LNAPL with Simulation High. The relatively good agreement of total LNAPL saturations between the model and simulations is because of the close agreement of free and entrapped LNAPL predictions with the model and simulations. The comparisons show the assumption made by Lenhard et al. (2017) that predicted free, entrapped, and residual LNAPL saturations will be similar whether the historical highest or lowest fluid levels in monitoring wells occurred first is reasonable.

Discussion

The predicted LNAPL distributions show saturations vary with elevation because LNAPL and water heads vary with elevation. Entrapped and residual saturations are not constant below and above the water-saturated zone as modeled by others (Charbeneau 2007; Jeong and Charbeneau 2014). Further, the Lenhard et al. (2017) model considers saturation path history. The distances between the current and historic fluid levels in wells reflect elevation-dependent saturation paths from which free, entrapped, and residual LNAPL saturations are calculated and used to predict the LNAPL relative permeability. The current LNAPL saturations (free, entrapped, and residual) and relative permeability at each elevation will be different depending on the elevations of the current fluid levels in a well relative to the historic levels.

The free LNAPL distribution represents potentially mobile LNAPL. The free LNAPL below Z_{ao} can potentially discharge into wells, provided permeable screening exists at those elevations, because the LNAPL head is greater than atmospheric. The free LNAPL above Z_{ao} will be under subatmospheric heads and will not flow into large cavities, such as wells, because of capillary forces. The free LNAPL, however, can migrate through the subsurface provided a horizontal LNAPL head gradient exists. The movement will be relatively slow because the LNAPL relative permeabilities decrease significantly with an increase in elevation above Z_{ao}. The residual LNAPL above Z_{ow} is predicted to be relatively immobile and possibly represents long-term sources for potential groundwater contamination. The residual LNAPL cannot be removed via LNAPL recovery operations (i.e., pumping LNAPL from wells). Partitioning into the gas phase, dissolving into the aqueous phase, and biodegradation can reduce the residual LNAPL.

The current fluid levels in wells will reflect the free LNAPL saturations and mobility after effects of historic fluid level fluctuations are considered. The historical highest levels (Z_{ao}^{max}) govern formation of residual LNAPL higher in the vadose zone. The historical lowest levels (Z_{ow}^{min}) govern formation of entrapped LNAPL in the water-saturated zone. As long as there is continuous connection between the fluids in a well (free LNAPL) and the subsurface, then the fluid levels in a well at static conditions can be used to predict LNAPL saturations and mobility in the subsurface. If there is not good contact because of any reason, then fluid levels in a well will not reflect LNAPL saturations and mobility in the subsurface. Achieving static conditions is not an absolute requirement, static conditions only need to be approached. In numerical multiphase simulators, constitutive relations among relative permeabilities, saturations, and capillary heads typically commonly employ parameters describing static conditions between fluid saturations and capillary heads.

An issue is older models for predicting LNAPL contents and mobility from measurements in wells were based on the knowledge of porous media physics at the time. With the passage of time, knowledge of porous media physics has improved and models based on the advanced knowledge may yield more accurate information. Therefore, LNAPL well measurements can be used to predict LNAPL saturations and mobility, but one must understand the conditions and if good contact between LNAPL in the well and the subsurface exists. Relying on older knowledge of porous media physics, some regulatory guidance may require remediation practitioners to attempt to cleanup more than "to the maximum extent practicable" based on newer knowledge and models.

Predictions of LNAPL saturations and relative permeabilities with the model can update conceptual site models of LNAPL contaminated sites and guide remediation strategy and activities. The well and other measurements over time can be used to refine model parameters to obtain more accurate predictions in the future to guide refinement of conceptual site models and remediation operations similar to how petroleum reservoir engineers use history matching (Chithra Chakra and Saraf 2016) to refine parameters of their predictive models.

Summary and Conclusion

To test an assumption made in a recent model by Lenhard et al. (2017) predicting free, entrapped, and residual LNAPL saturations and transmissivity in the subsurface from measurements of fluid levels in wells after accounting for effects of historic fluid level fluctuations, simulations were conducted with a modified multiphase flow numerical simulator TMVOC and compared to results from the model. The assumption is the predicted free, entrapped, and residual LNAPL distributions will not be very different whether the historical highest fluid levels in a well or the historical lowest fluid levels in a well occur first. The basis for the assumption was the historical highest fluid levels govern establishment of residual LNAPL, the historical lowest fluid levels govern establishment of entrapped LNAPL, and the current fluid levels largely govern the free LNAPL.

The simulations using TMVOC utilized the same LNAPL constitutive relative permeability-saturation-capillary head relations in the Lenhard et al. (2017) model. In one simulation, the initial condition reflected fluid levels in a well at the historical highest elevations. In the other simulation, the initial condition reflected fluid levels in a well at the historical lowest elevations. Thereafter, the boundary conditions were changed so conditions reflecting the historical lowest or highest fluid level elevations would result, depending on the initial condition. Afterward, the boundary conditions were changed to reflect conditions consistent with the current fluid levels in a well.

Comparisons of the free, entrapped, residual, and total LNAPL saturations from the simulations and the Lenhard et al. (2017) model showed good agreement, except for the residual LNAPL with the initial condition reflecting the historical highest fluid level elevations. The lack of agreement was explained because a larger LNAPL volume was present for that simulation when the residual LNAPL was created than for the other simulation and the model. The larger volume was needed because of how initial conditions are implemented in TMVOC. The predicted free LNAPL saturations from both simulations and the model are in good agreement. Therefore, it appears as if the assumption made by Lenhard et al. (2017) for predicting free, entrapped, and residual LNAPL distributions using current and historical fluid levels in monitoring wells is reasonable.

The Lenhard et al. (2017) model is useful for communicating detailed and complicated LNAPL distributions in an easy and understandable format to assist in developing conceptual site models, remediation strategies, and assessing current conditions and potential risks. A constraint is the assumed vertical hydrostatic condition. While it may take hours to prepare and predict fluid distributions with numerical simulators, it takes a second for the Lenhard et al. (2017) model. Practitioners can assess whether a technical impracticability in recovering LNAPL from the subsurface may exist with the model using fundamental principles. Further, regulatory agencies can assess whether LNAPL recovery has likely reached a technology endpoint and assess potential risks of LNAPL migration as a non-aqueous liquid. The Lenhard et al. (2017) model is appropriate for assessing potential subsurface LNAPL volumes and transmissivity from current and historical fluid levels in nearby wells. For more complicated investigations focusing on multicomponent transport of LNAPL compounds, then a numerical model like the modified TMVOC is appropriate. In the paper, we described an approach to include LNAPL constitutive relative permeability-saturation-capillary head relations from the Lenhard et al. (2017) model into TMVOC.

Acknowledgments

The work has been supported by the Cooperative Research Centre for Contamination Assessment and Remediation of the Environment (CRC CARE), whose activities are funded by the Australian Government's Cooperative Research Centers Programme.

References

ASTM. 2013. *Standard Guide for Estimation of LNAPL Transmissivity. E2856-13*. West Conshohocken, Pennsylvania: ATSM International.

Charbeneau, R.J. 2007. *LNAPL Distribution and Recovery Model (LDRM). Volume 1: Distribution and Recovery of Petroleum Hydrocarbon Liquids in Porous Media*. API Publ. No. 4760. Washington, DC: American Petroleum Institute.

Chithra Chakra, N.C., and D.N. Saraf. 2016. History matching of petroleum reservoirs employing adaptive genetic algorithm. *Journal of Petroleum Exploration and Production Technology* 6: 653–674.

CRC CARE. 2015. A practitioner's guide for the analysis, management and remediation of LNAPL. CRC CARE Technical Report 34. Adelaide, Australia: CRC for Contamination Assessment and Remediation of the Environment.

Farr, A.M., R.J. Houghtalen, and D.B. McWhorter. 1990. Volume estimation of light nonaqueous phase liquids in porous media. *Groundwater* 28: 48–56.

van Genuchten, M.T. 1980. A closed-form equation for predicting the hydraulic conductivity of unsaturated soils. *Soil Science Society of America* 44: 892–898.

Jeong, J., and R.J. Charbeneau. 2014. An analytical model for predicting LNAPL distribution and recovery from multi-layered soils. *Journal of Contaminant Hydrology* 156: 52–61.

Lekmine, G., K. Sookhak Lari, C.D. Johnston, T.P. Bastow, J.L. Rayner, and G.B. Davis. 2017. Evaluating the reliability of equilibrium dissolution assumption from residual gasoline in contact with water saturated sands. *Journal of Contaminant Hydrology* 196: 30–42. https://doi.org/10.1016/j.jconhyd.2016.12.003

Lenhard, R.J., and J.C. Parker. 1987. A model for hysteretic constitutive relations governing multiphase flow, 2. Permeability-saturation relations. *Water Resources Research* 23: 2197–2206.

Lenhard, R.J., and J.C. Parker. 1990a. Estimation of free hydrocarbon volume form fluid levels in monitoring wells. *Groundwater* 28: 57–67.

Lenhard, R.J., and J.C. Parker. 1990b. Discussion of estimation of free hydrocarbon volume form fluid levels in monitoring wells. *Groundwater* 28: 800–801.

Lenhard, R.J., M. Oostrom, and J.H. Dane. 2004. A constitutive model for air-NAPL-water flow in the vadose zone accounting for immobile, non-occluded (residual) NAPL in strongly water-wet porous media. *Journal of Contaminant Hydrology* 73: 283–304.

Lenhard, R.J., J.L. Rayner, and G.B. Davis. 2017. A practical tool for estimating subsurface LNAPL distributions and transmissivity using current and historical fluid levels in groundwater wells: Effects of entrapped and residual LNAPL. *Journal of Contaminant Hydrology* 205: 1–11. https://doi.org/10.1016/j.jconhyd.2017.06.002

MassDEP. 2016. Final policy #WSC-16-450 light nonaqueous phase liquid and the MCP: Guidance on site assessment and closure February 2016. Massachusetts Department of Environmental Protection. Boston, MA, February 2016, 53 pp.

MDEQ. 2014. Non-aqueous phase liquid (NAPL) characterization, remediation, and management for petroleum releases. Michigan Department of Environmental Quality, Remediation and Redevelopment Division. Lansing, MI. RRD Resource Materials-25-2014-01. June 2014, 21 pp.

Montana DEQ. 2013. Montana light non-aqueous phase liquid (LNAPL) recovery and monitoring guidance. Montana Department of Environmental Quality, Remediation Division, July 2013, 26 pp.

NJDEP. 2012. Light non-aqueous phase liquid (LNAPL) initial recovery and interim remedial measures technical guidance. New Jersey Department of Environmental Protection, June 2012, 33 pp.

Oostrom, M., M.D. White, R.J. Lenhard, P.J. van Geel, and T.W. Wietsma. 2005. A comparison of models describing residual NAPL formation in the vadose zone. *Vadose Zone Journal* 4: 163–174.

Parker, J.C., and R.J. Lenhard. 1987. A model for hysteretic constitutive relations governing multiphase flow, 1. Saturation-pressure relations. *Water Resources Research* 23: 2187–2196.

Parker, J.C., R.J. Lenhard, and T. Kuppusamy. 1987. A parametric model for constitutive properties governing multiphase flow in porous media. *Water Resources Research* 23: 618–624.

Parker, J.C., J.J. Kaluarachchi, V.J. Kremesec, and E.L. Hockman. 1990. Modeling free product recovery at hydrocarbon spill sites. In: *Conference of Petroleum Hydrocarbons and Organic Chemicals in Ground Water: Prevention,* Detection and Restoration, National Water Well Association, 641–655.

Parker, J.C., J.L. Zhu, T.G. Johnson, V.J. Kremesec, and E.L. Hockman. 1994. Modeling free product migration and recovery at hydrocarbon spill sites. *Groundwater* 32: 119–128.

Pruess, K., and A. Battistelli. 2002 *TMVOC, A Numerical Simulator for Three-Phase Non-isothermal Flows of Multicomponent Hydrocarbon Mixtures in Saturated-Unsaturated Heterogeneous Media*, 2.1 ed. Berkeley, California: Lawrence Berkeley National Laboratory.

Sookhak Lari, K., G.B. Davis, and C.D. Johnston. 2016a. Incorporating hysteresis in a multi-phase multi-component NAPL modelling framework; A multi-component LNAPL gasoline example. *Advances in Water Resources* 96: 190–201. https://doi.org/10.1016/j.advwatres.2016.07.012

Sookhak Lari, K., C.D. Johnston, and G.B. Davis. 2016b. Gasoline multi-phase and multi-component partitioning in the vadose zone: Dynamics and risk longevity. *Vadose Zone Journal* 15: 1–15. https://doi.org/10.2136/vzj2015.07.0100

Suthersan, S.S., S.T. Potter, M. Schnobrich, J. Wahlberg, J. Guinnan, N. Welty, and T. Fewless. 2016. Rethinking conceptual site models in groundwater remediation. *Journal of Groundwater Monitoring & Remediation* 36, no. 4: 22–30.

US EPA. 1988. Underground storage tanks; technical requirements and state program approval; final rules. 53 Federal Register 37082-37247, September 23, 1988, 40 CFR Parts 280 and 281.

US EPA. 2004. A decision-making framework for cleanup of sites impacted with light non-aqueous phase liquids (LNAPL). EPA 542-R-04-011. https://www.epa.gov/remedytech/decision-making-framework-cleanup-sites-impacted-light-non-aqueous-phase-liquids-lnapl

VDEQ. 2012. Storage tank program: Case closure evaluation of sites with free product. Department of Environmental Quality, Office of Spill Response and Remediation. Document Number LPR-SRR-0302012, December 2012, 11 pp.

Waddill, D.W., and J.C. Parker. 1997. Simulated recovery of light, nonaqueoous phase liquid from unconfined heterogeneous aquifers. *Groundwater* 35: 938–947.

Biographical Sketches

***R.J. Lenhard**, Ph.D., corresponding author, multiphase flow/soil physicist, San Antonio, Texas, USA; rj.lenhard@yahoo.com*

***Kaveh Sookhak Lari**, Ph.D., DIC, is a computational fluid dynamics scientist, CSIRO Land & Water, Private Bag 5, Wembley, WA 6913 Australia; Kaveh.Sookhaklari@csiro.au; an adjunct lecturer, School of Engineering, Edith Cowan University, 270 Joondalup Drive, Joondalup, WA 6027, Australia; and associated with the Cooperative Research Centre for Contamination Assessment and Remediation of the Environment (CRC CARE), Australia.*

***J.L. Rayner**, is a Team Leader, CSIRO Land & Water, Private Bag 5, Wembley, WA 6913 Australia; John.Rayner@csiro.au; and associated with the Cooperative Research Centre for Contamination Assessment and Remediation of the Environment (CRC CARE), Australia.*

***G.B. Davis**, Ph.D., is a Research Director, CSIRO Land & Water, Private Bag 5, Wembley, WA 6913 Australia; Greg.Davis@csiro.au; an adjunct professor, School of Earth and Environment, The University of Western Australia, 35 Stirling Highway Crawley, WA 6009, Australia; and associated with the Cooperative Research Centre for Contamination Assessment and Remediation of the Environment (CRC CARE), Australia.*